HHS Public Access

Author manuscript

Nat Struct Mol Biol. Author manuscript; available in PMC 2015 June 01.

Published in final edited form as:

Nat Struct Mol Biol. 2014 December ; 21(12): 1058–1067. doi:10.1038/nsmb.2922.

Stapled HIV-1 Peptides Recapitulate Antigenic Structures and Engage Broadly Neutralizing Antibodies

Gregory H. Bird[1,2,3,‡], **Adriana Irimia**[4,5,6,‡], **Gilad Ofek**[7], **Peter D. Kwong**[7], **Ian A. Wilson**[4,5,6], and **Loren D. Walensky**[1,2,3,*]

[1]Department of Pediatric Oncology, Dana-Farber Cancer Institute, Boston, MA, USA

[2]Division of Hematology/Oncology, Boston Children's Hospital, Boston, MA, USA

[3]Department of Pediatrics, Harvard Medical School, Boston, MA, USA

[4]Department of Integrative Structural and Computational Biology, The Scripps Research Institute, La Jolla, CA, USA

[5]International AIDS Vaccine Initiative Neutralizing Antibody Center, The Scripps Research Institute, La Jolla, CA, USA

[6]Scripps Center for HIV/AIDS Vaccine Immunology and Immunogen Discovery, The Scripps Research Institute, La Jolla, CA, USA

[7]Vaccine Research Center, National Institutes of Allergy and Infectious Diseases, National Institutes of Health, Bethesda, MD, USA

Abstract

Hydrocarbon stapling can restore bioactive, α-helical structure to natural peptides, yielding research tools and prototype therapeutics to dissect and target protein interactions. Here, we explore the capacity of peptide stapling to generate high fidelity, protease-resistant mimics of antigenic structures for vaccine development. HIV-1 has been refractory to vaccine technologies thus far, although select human antibodies can broadly neutralize HIV-1 by targeting sequences of the gp41 juxtamembrane fusion apparatus. To develop candidate HIV-1 immunogens, we generated and characterized stabilized α-helices of the membrane proximal external region (SAH-

*To whom correspondence should be addressed: Loren D. Walensky, Dana-Farber Cancer Institute, 450 Brookline Ave, Mayer 664, Boston, MA 02215, Phone: (617) 632-6307, Fax: (617) 582-8240, Loren_Walensky@dfci.harvard.edu.
‡these authors contributed equally to the work

ACCESSION CODES

The atomic coordinates and structure factors of the 4E10 Fab–SAH-MPER$_{(671\text{-}683KKK)}$(q), 4E10 Fab–SAH-MPER$_{(671\text{-}683KKK)}$(q)pSer, and 10E8 Fab–SAH-MPER$_{(662\text{-}683KKK)}$(B,q) complexes have been deposited in the Protein Data Bank, with the accession codes 4NHC, 4NGH and 4U6G, respectively.

AUTHOR CONTRIBUTIONS

G.H.B. and L.D.W. designed, synthesized, and characterized SAH-MPER peptides, and conducted the antibody-binding, peptide proteolysis, and mass spectrometry analyses, A.I. and I.A.W. performed the structural studies of the 4E10 Fab–SAH-MPER complexes, and G.O. and P.D.K conducted the structural analysis of the 10E8 Fab–SAH-MPER complex. L.D.W. wrote the manuscript with contributions from all authors.

COMPETING FINANCIAL INTERESTS

L.D.W. is a scientific advisory board member and consultant for Aileron Therapeutics.

MPER) of gp41. SAH-MPER peptides were remarkably protease-resistant and bound to the broadly neutralizing 4E10 and 10E8 antibodies with high affinity, recapitulating the structure of the MPER epitope when differentially engaged by the two anti-HIV Fabs. Thus, stapled peptides may provide a new opportunity to develop chemically-stabilized antigens for vaccination.

INTRODUCTION

Antibodies neutralize pathogens by recognizing discrete and distinguishing peptidic motifs. By presenting primary, secondary, and tertiary structures to the host immune system, vaccines have revolutionized our capacity to prevent human infection. Nevertheless, some targets, such as human immunodeficiency virus type 1 (HIV-1), have been refractory to vaccine development. To achieve sterilizing HIV-1 immunity, an effective vaccine must elicit broadly neutralizing antibodies that intercept the virus prior to immune cell penetrance[1]. Upon interaction of the HIV-1 envelope (Env) glycoprotein with host receptors, the Env viral fusion protein undergoes a series of conformational changes that are essential to penetrating the plasma membrane and fusing the viral and host membranes. Three copies of the HIV-1 envelope glycoproteins gp120 and gp41, which are non-covalently associated, form the Env trimer[2]. Once gp120 binds to CD4[3] and co-receptor[4] on the host cell membrane, gp41 transforms from its metastable native state into a fusogenic six-helix bundle[5,6] that conjoins viral and host cell membranes, enabling viral particle uptake. The regions of gp41 involved in this structural reorganization are the N-terminal heptad repeat (HR1) found just downstream of the fusion peptide and the C-terminal heptad repeat (HR2) that is close to the transmembrane region. The membrane-proximal external region[7] (MPER) is downstream from HR2 and contains antigenic sequences recognized by several broadly neutralizing human antibodies, including 2F5[7], Z13e1[8], 4E10[9], and 10E8[10].

Structural studies have identified critical motifs in gp41 that engage broadly neutralizing antibodies[10–17]. The crystal structure of 4E10 fragment antigen-binding (Fab) in complex with a 13-residue portion of the MPER (amino acids 671-683) demonstrated that this peptide epitope adopts an α-helical conformation. Residues W672-D674 are configured as a short 3_{10} helix that directs the N-terminus out of the binding site[18] and the interaction surface is comprised of key residues W672, F673, I675, and T676[12]. Analysis of a longer 22-residue MPER peptide (amino acids 662-683) in a lipid context, using a combination of nuclear magnetic resonance (NMR) and electron paramagnetic resonance (EPR) spectroscopy, revealed a unique L-shaped structure, reflecting a bipartite α-helix segmented by a kink[17]. The 10E8 antibody also recognizes an extended MPER peptide (amino acids 656-683) in a helix-kink-helix conformation, with each αhelix oriented 100° relative to the other[10]. In contrast, 2F5 binds to its target MPER sequences in a largely extended conformation with a central β-turn[16]. Importantly, upstream α-helical HR2 sequences, the transmembrane domain, the trimeric nature of the viral spike, and the plasma membrane itself may provide an important structural context that constrains and thereby helps define the neutralization-competent antigenic structure(s) of the MPER[19].

Diverse approaches have been applied to display the MPER domain for vaccine development, including computational design of epitope scaffolds[20–24], MPER grafting[25],

use of chimeric viruses[26], and immunizing with cells expressing the gp41 post-fusion complex[27]. Despite these efforts, non-neutralizing responses are the norm[23–25]. The conformations and orientations of MPER sequences displayed on the surface of nanoparticles[28], rhinovirus[26], or human cells[27] may be distinct from the pathologic epitope *in vivo* or elicit off-target immune responses to the scaffold itself. Peptidic approaches to MPER mimicry have also been unsuccessful to date, potentially due to limitations in peptide size, stability, and delivery, as documented for peptide vaccine studies in general[29–31].

Introduction of non-covalent or covalent constraints to stabilize variably-structured MPER sequences of different length has enhanced binding to select broadly neutralizing antibodies, but did not necessarily elicit a broadly neutralizing response.[32,33] These data suggest that perhaps an MPER motif of optimal size or structure in the appropriate context (such as the membrane environment) was not reproduced, or structural integrity was not maintained *in vivo* due to proteolysis. We have found for structured therapeutic peptides that non-covalently constrained constructs are rapidly proteolyzed[34], and covalently-constrained peptides bearing labile crosslinks (e.g. disulfides, amides) are also vulnerable. Indeed, the structural lability of the Env trimer itself was recently shown to be a critical factor in eliciting non-neutralizing anti-HIV-1 antibodies[35]. Although broadly neutralizing antibodies that target the HIV-1 envelope are among the most protective for preventing HIV-1 transmission, the requisite set of immunogens to appropriately guide an effective immune response has been elusive to date[36].

Two of the historically most broadly neutralizing monoclonal antibodies, 2F5 and 4E10, have been proposed to cross-react with self-antigens[37–42], raising the specter of autoreactivity as an unwanted consequence of a potential MPER-based vaccine. To preclude autoreactivity, a normal immune response may not permit the emergence of MPER-directed neutralizing antibodies. Such concerns, however, have been mitigated by the recent discovery of 10E8, a potent and broadly neutralizing antibody that also engages a helical MPER, but without autoantigen recognition[10], providing a compelling basis for revisiting an MPER-based vaccine strategy. Interestingly, a recent follow-up study demonstrated that 10E8 retains weak affinity for lipid membranes and suggested a functional role for apical residues of its complementarity determining region (CDR)-H3 in membrane binding and viral neutralization[43], as also observed for 2F5[21] and 4E10[20]. Taken together, these studies indicate that effective HIV-1 neutralization by MPER-specific antibodies mechanistically involves interactions with viral lipids[16,20,21,43], yet structural delineation of the lipid binding site(s) on MPER antibodies is lacking. Ultimately, structured MPER peptides presented in a lipid context or MPER-based antigens designed to contain lipid recognition moieties may be ideally suited for vaccine development[43].

Motivated by fresh insights into the conformation of MPER epitopes in the membrane context[17] and in complex with potent and broadly neutralizing antibodies[10], we sought to design stabilized α-helices of MPER domains (SAH-MPERs) that reflect the full-length domain, reinforcing both helical components of the helix-kink-helix structure. Our peptide stapling method has yielded remarkably protease-resistant α-helical peptides[34], transforming tool reagents into prototype therapeutics with *in vivo* efficacy[44–47]. Importantly, the all-hydrocarbon constraint is itself protease-resistant, differentiating this chemical approach

from prior peptide-stabilization efforts and potentially rendering it well-suited for the development of structured antigens in general. Here, we demonstrate that SAH-MPER peptides retain high affinity binding activity toward two broadly neutralizing anti-HIV-1 antibodies, exhibit markedly enhanced protease resistance, and recapitulate the critical antibody recognition motif, as evidenced by crystal structures of the corresponding 4E10 and 10E8 complexes.

RESULTS

Design and 4E10-binding Activity of SAH-MPER Peptides

To generate candidate HIV-1 immunogens with neutralization-competent structure, we sought to replicate the bipartite α-helical conformation of the full-length MPER domain (Fig. 1a). To independently stabilize the respective N- (662-671) and C- (675-683) terminal helices, which are separated by a flexible hinge region (672-674), we performed staple scans in each region of the MPER peptide. Pairs of (S)-2-(((9H-fluoren-9-yl)methoxy)carbonylamino)-2-methyl-hept-6-enoic acids (abbreviated as S5 residues) were substituted at *i, i+4* positions within the N-terminal region followed by ruthenium-catalyzed ring-closing metathesis (RCM) to generate six single-stapled peptides, termed SAH-MPER$_{(662\text{-}683)}$ A through F (Fig. 1b, Supplementary Table 1). Within the C-terminal region, *i, i+4* and *i, i+3* substitutions were made in order to accommodate α- or 3_{10}-helical conformation, yielding thirteen single-stapled peptides, termed SAH-MPER$_{(662\text{-}683)}$ G-L (*i, i+4*) and M-S (*i, i+3*) (Fig. 1c). Of note, *i, i+3* hydrocarbon stapling of S5 residues required a prolonged reaction time at elevated temperature to achieve yields similar to the traditional *i, i+4* reaction, consistent with pentane interference from the resultant crosslink that drapes over the N-terminal α-methyl group[48].

We compared the binding activity of 4E10 antibody across our diversity of hydrocarbon-stapled peptides by competitive enzyme-linked immunosorbent assay (ELISA), pitting the unmodified MPER peptide (amino acids 662-683) against FITC-labeled competitor constructs. Whereas the affinity-driving contacts of 4E10 are on the C-terminal half of the MPER peptide[12], we chose to incorporate N-terminal MPER sequence into our designs to maximize their potential immunogenic surface. Among the N-terminal *i, i+4* stapled constructs, all but the most C-terminal F staple was tolerated, consistent with this N-terminal portion of the MPER domain lying outside the core 4E10-binding region and staple encroachment on the kink region being disfavored (Fig. 1b). Among the C-terminal *i, i+4* and *i, i+3* stapled constructs, only two constructs showed 4E10 binding activity. In each case, the favorable staple localized to the non-interacting helical surface and centered around the highly conserved L679-W680 motif. The C-terminal *i, i+4* staple K conferred a 3-fold improvement in 4E10 binding activity, whereas the *i, i+3* staple Q yielded a 60-fold enhancement (Fig. 1c). The exquisite sensitivity of 4E10-binding activity to staple location emphasizes the importance of staple scanning to identify insertion points that balance structural reinforcement and preservation of key residues and binding interfaces.

To reinforce both helical motifs that flank the kink and maximize protease resistance[34], we sought to generate double-stapled peptides, combining the C-terminal *i, i+3* Q staple with those N-terminal staple positions that yielded similar or improved 4E10 binding activity (A–

E). However, the designed (*i, i+4*), (*i, i+3*) MPER constructs either failed to metathesize or resulted in minimal yield even after prolonged reaction at elevated temperatures, consistent with the requirement for relatively extreme conditions to accomplish single *i, i+3* stapling with S5. These results compelled us to determine which alternative non-natural olefin-bearing amino acids would enable *i, i+3* stapling to proceed as smoothly as single and double *i, i+4* stapling with S5[34].

Optimization of *i, i+3* Stapling for SAH-MPER Design

We tested the reactivity of an alternative stapling amino acid pair in order to optimize *i, i+3* stapling for SAH-MPER synthesis. For a simplified peptide template, we used the previously described 4E10-binding epitope that corresponds to the C-terminal half of the MPER domain with an appended trio of lysines to enhance solubility[18] (hereafter referred to as $MPER_{(671\text{-}683KKK)}$). S5 residues were installed at positions 678 and 681 and the resin-bound peptide exposed to ruthenium-catalyzed RCM for 2 h at room temperature, with no observed metathesis (data not shown). The reaction conditions were then escalated to an 18 h incubation at 84°C (reflux in dichloroethane) and only 20% conversion was achieved, as demonstrated by an overlay of the high performance liquid chromatography (HPLC) traces of starting material and reaction product (Fig. 2a). We reasoned that shortening the alkenyl side chain of one of the amino acids from 5 to 3 carbons and inverting the more N-terminal stereocenter would mitigate steric hindrance and orient the olefins toward each other. Therefore, we installed an S5 residue at position 681 and an R3 residue, (R)-2-(((9H-fluoren-9-yl)methoxy)carbonylamino)-2-methyl-pent-4-enoic acid, at position 678. Remarkably, we achieved almost complete conversion of the starting material into metathesized product with only 2 h incubation at room temperature, matching the synthetic efficiency of *i, i+4* stapling with two S5 residues (Fig. 2b). Consistent with the enhanced 4E10 binding affinity derived from S5-S5 stapling at the Q position of the full-length MPER peptide, R3-S5 stapling of the 671-683KKK construct at position Q (designated q to reflect the alternate staple composition) resulted in 5-fold improvement in competitive binding activity compared to the unmodified $MPER_{(671\text{-}683KKK)}$ peptide (Fig. 2c).

Crystal Structure of a Stapled MPER Peptide Bound to 4E10

We determined the crystal structure of the 4E10 Fab–SAH-$MPER_{(671\text{-}683KKK)}$(q) complex at 2.9 Å resolution with one Fab–peptide complex per asymmetric unit (Fig. 3a, Table 1). With the exception of the C-terminal lysine side chains, all main chain and side chains of the stapled peptide residues could be modeled into the electron density map (Fig. 3b). The relatively weak electron density for the region of the 6-atom carbon staple, which replaced the side chains of W678 and Y681, could not distinguish between *Z* and *E* olefin isomers (or exclude the possibility of a stereoisomeric mixture), and was modeled in a *Z* conformation in this 2.9 Å structure. Density appears for most of the main chain of the flexible complementarity-determining region (CDR)-H3 loop (residues 99-100D, except $W100^{(H)}$ and $G100A^{(H)}$) (Supplementary Fig. 1a)[18]. The complexes of 4E10 Fab with SAH-$MPER_{(671\text{-}683KKK)}$(q) and the original (unmodified) 4E10-epitope peptide (PDB 2FX7)[18] superimpose with a root-mean-square-deviation of 0.73 Å for the Cα atoms, and are overall very similar (Supplementary Fig. 1b). Superimposing the peptide regions revealed essentially identical Fab-binding interfaces, highlighting that the q staple reinforces the

natural peptide-bound structure (Fig. 3c). Like the side chains of W678 and Y681, the 6-carbon staple that replaces these natural residues does not contact the antibody due its location on the solvent-exposed face of the helical peptide. Thus, hydrocarbon stapling effectively recapitulates the native antigenic epitope, with the structurally-reinforcing staple positioned away from, and thereby not perturbing, the critical binding interface.

Identification of a Phosphate Binding Site on 4E10

The MPER-specific antibodies 2F5 and 4E10 can also bind several phospholipid antigens[39]. The initial difference Fourier electron density map of our 4E10 Fab–SAH-MPER$_{(671\text{-}683KKK)}$(q) complex revealed roughly spherical electron density of approximately 7σ located between S28H and S30H of the CDR-H1 loop (Fig. 4a, 4b). Both phosphate and chloride ions were present in the crystallization conditions (based on mother liquor conditions that contained sodium and potassium phosphate [0.1 M] and sodium chloride [0.2 M]). When a chloride ion was refined into the extra density, residual positive electron density still remained in Fo-Fc maps. Thus, the spherical density was interpreted as a phosphate ion, which fits the density with a real space correlation coefficient of 0.96. Although the B-value for the phosphate ion is high (~110 Å^2, Table 1) compared to the overall protein, it is nevertheless close to that of neighboring CDR-H1 residues (*ca.* 90 Å^2 for S28$^{(H)}$, 74 Å^2 for F29$^{(H)}$ and 83 Å^2 for S30$^{(H)}$; Fig. 4b). Elevated isotropic B-values were also observed for these CDR-H1 loop residues in the previous 4E10 Fab–SAH-MPER$_{(671\text{-}683KKK)}$ structure in comparison to mean isotropic and Wilson B-values at the corresponding resolution[18], and suggests increased structural flexibility. The superimposition of the phosphate-incorporated site with the same region in the 4E10 Fab–native MPER$_{(671\text{-}683KKK)}$ complex (PDB entry 2FX7)[18], which was crystallized from phosphate-free buffer, demonstrates torqueing of backbone amides and reorientation of the S28$^{(H)}$ hydroxyl toward the phosphate ion to promote favorable hydrogen bond interactions in the 4E10 Fab–SAH-MPER$_{(671\text{-}683KKK)}$(q) structure (Fig. 4c). The presence of a phosphate binding site in the CDR-H1 loop region of 4E10 is consistent with antibody binding to anionic lipids at the membrane surface. Indeed, the orientation of SAH-MPER$_{(671\text{-}683KKK)}$(q) within the antigen binding site positions the C-terminal residues 684-686, which are replaced here by lysines and would comprise the start of the gp41 transmembrane segment, immediately adjacent to the identified phosphate-binding site (Fig. 4a).

To our knowledge, we have detected this phosphate-binding site in the 4E10 combining region for the first time, as a PDB search of all available 4E10 structures did not reveal phosphate as a buffer component of prior crystallization conditions. A recent crystal structure of the 4E10 variable region (Fv) in an unliganded form[49] shows sulfate ions near the CDR-H1 loop, but none of the ions are in the same position as observed here for the phosphate. In fact, a glycerol molecule is present in this position in one of the four Fv molecules in the asymmetric unit. Whereas sulfate and phosphate ions are similar, and can occupy the same binding site in a protein, the peptide-free structure of 4E10[49] has its CDR-H1 and CDR-H3 loops drastically perturbed compared to the peptide-bound form[18]. In the unliganded structure, the CDR-H3 occupies the peptide binding site but is also involved in extensive packing interactions with symmetry-related mates. It is also noteworthy that the

acidic pH of 4.6 and the high salt concentration (0.4–0.8 M Li_2SO_4) in the crystals could impact the conformation. To avoid exposure of the hydrophobic residues in the combining site, which otherwise interacts with the MPER, the CDR-H3 loop forms extensive packing interactions with symmetry-related mates and residues of the peptide binding-site. Thus, the disposition of the phosphate ion reported here in the liganded structure in the CDR-H1 of 4E10 could indeed reflect a 4E10 membrane-binding interface. That said, we do not exclude participation of the hydrophobic CDR-H3 in membrane lipid interactions, as reported for 2F5[16,21], 4E10[20], and 10E8[43].

Crystal Structure of 4E10 and a SAH-MPER Phosphopeptide

To probe the potential role of phosphate-engagement as a 4E10 binding determinant at the membrane, we generated a modified SAH-$MPER_{(671\text{-}683KKK)}$(q) peptide containing a tethered phosphate moiety. Based on the predicted 5.5 Å distance between the K683 side-chain amine and phosphate group (Fig. 4a), we modeled in a phosphoserine (pSer) group and determined that it could be appropriately linked to the peptide backbone by a diaminobutanoic acid and glycine (Dab683-Gly) spacer (Fig. 5a). We then synthesized SAH-$MPER_{(671\text{-}683KKK)}$(q) containing the Dab-Gly-pSer tether at the 683 position or, as a negative control, at the 685 position, which would orient pSer away from the binding interface (Supplementary Fig. 2a). Competitive 4E10 binding analysis revealed a slight improvement in binding affinity upon incorporation of a phosphate moiety at position 683, whereas installing the equivalent derivatization at position 685 actually reduced binding activity (Supplementary Fig. 2b).

To confirm that the installed phosphate moiety at position 683 interacted with the defined phosphate-binding site at the 4E10 interface, we undertook structural analysis of the 4E10 Fab bound to phosphate-derivatized SAH-$MPER_{(671\text{-}683KKK)}$(q)pSer peptide containing the Dab-Gly spacer. The structure of the complex was determined at 2.68 Å resolution from a crystal grown in phosphate-free mother liquor (Fig. 5b). The initial difference Fourier map shows unambiguous positive electron density for the covalently-linked staple, which fit the electron density with a real space correlation coefficient of 0.98 and an isotropic B-value of 49 $Å^2$, in good agreement with the Wilson plot and mean isotropic B values (Table 1; Supplementary Fig. 3a, 3b). In contrast, the initial positive Fo-Fc (3σ level) and the 2Fo-Fc (1σ level) maps show incomplete electron density for the central portion of the Dab-Gly linker (Supplementary Fig. 4a). However, the final 2Fo-Fc density at the Dab level (Supplementary Fig. 4b) improved after refinement compared with the density for the SAH-$MPER_{(671\text{-}683KKK)}$(q) K683 (Fig. 4b) or with the density for the same lysine in the 1.76 Å structure of native $MPER_{(671\text{-}683KKK)}$ in complex with 4E10 (PDB entry 2FX7)[18], where density was observed only for the main chain. With the exception of two atoms (OZ1 and N6), all of the atoms of the Dab-Gly-pSer are located inside the 2Fo-Fc electron density map at the 0.8σ level (Supplementary Fig. 4c). Therefore, the strong density (5σ level in the initial Fo-Fc map) for the phosphate moiety and the improved density at the Dab level, combined with the absence of phosphate in the mother liquor, indicate that the Dab-Gly-pSer tether at position 683 extends into the phosphate-binding site (Fig. 5b, 5c and Supplementary Fig. 4d). However, for the linker atoms that connect the peptide backbone to the phosphate moiety, reduced density for the eight-atom linker and a high isotropic B-value

of approximately 112 Å^2 (*ca.* 105 Å^2 for the whole Dab-Gly-pSer residue, Table 1) is observed, indicative of its flexibility. The 4E10 Fab complexes with SAH-MPER$_{(671\text{-}683KKK)}$(q)pSer and SAH-MPER$_{(671\text{-}683KKK)}$(q) are otherwise very similar with only 0.23 Å r.m.s. deviation (all Cα atoms) for the Fab and 0.17 Å r.m.s. deviation (all Cα atoms) for the corresponding peptides (Supplementary Fig. 1b and Supplementary Fig. 3c).

Potency and Stability of Double-stapled MPER Epitopes

The small size of the MPER$_{(671\text{-}683KKK)}$ template, limited sites for installing staples, along with its rapid proteolysis (Supplementary Fig. 5) continued to render (*i, i+4*), (*i, i+3*) double stapling of the extended MPER peptide the most compelling design to maximize immunogenic surface, reinforce neutralization-competent structure, and ensure protease resistance. Applying R3-S5 (*i, i+3*) and S5-S5 (*i, i+4*) stapling, all five doubly constructs were successfully generated using the standard 4 h, room temperature metathesis conditions (Fig. 6a). Competitive 4E10 binding analysis demonstrated IC$_{50}$s in the 130–600 nM range for double-stapled SAH-MPER$_{(662\text{-}683)}$ peptides. The best binder, SAH-MPER$_{(662\text{-}683)}$(D,q), nearly matched the binding activity of the corresponding single-stapled SAH-MPER$_{(662\text{-}683)}$(q) construct (132 nM vs. 91 nM, respectively), in which the 4E10-binding determinant (amino acids 671-683) is optimally stabilized by an *i, i+3* staple at positions 678 and 681 (Fig. 6a).

To interrogate the relative protease resistance of double-stapled SAH-MPER constructs, peptides were subjected to chymotrypsin proteolysis and the time-dependent degradation of full-length SAH-MPER was monitored by HPLC-mass spectrometry (MS). Because the double-stapled SAH-MPER$_{(662\text{-}683)}$ constructs ionized poorly upon MS analysis, the library of constructs was also synthesized with C-terminal KKK tails, which increased ionization potential and facilitated detection of a greater breadth of fragment ions. As observed for the corresponding unmodified and q-stapled MPER$_{(671\text{-}683KKK)}$ constructs (Supplementary Fig. 5), the unmodified and q-stapled full-length MPER$_{(662\text{-}683KKK)}$ peptides showed similar, rapid proteolysis profiles (Fig. 6b). In contrast, the introduction of double staples into the MPER$_{(662\text{-}683KKK)}$ sequence prolonged the proteolytic half-life by approximately 10- to 90-fold compared to the corresponding unstapled construct (Fig. 6b). Of the eight chymotrypsin proteolysis sites observed for the unmodified peptide, the most stable double-stapled SAH-MPERs eliminated the capacity of chymotrypsin to cleave all but one of them (Fig. 6c, Supplementary Fig. 6). Indeed, those chymotrypsin sites flanked by staples or located immediately adjacent to staples were completely shielded from proteolysis (Supplementary Fig. 6). Thus, at the expense of only a minor decrease in binding activity relative to the single-stapled SAH-MPER$_{(662\text{-}683)}$(q) construct (1.4-fold), the double-stapled SAH-MPER$_{(662\text{-}683)}$(D,q) peptide, for example, achieves a 140-fold increase in chymotrypsin resistance. Although here we initially used 4E10 binding activity as a guide for candidate immunogen design, it is important to note that the variety of MPER-specific neutralizing antibodies identified to date recognize a spectrum of peptide templates and conformations. Thus, in addition to the 4E10-optimized double-stapled MPER peptides (Fig. 6a), constructs that do not engage 4E10 (Fig. 1b, 1c) could potentially represent a library of alternatively structured yet highly stable MPERs for immunization.

Engagement of Double-stapled MPER Peptides by 10E8

The recent discovery of the 10E8 broadly neutralizing HIV-1 antibody[10] provided a unique opportunity to explore the binding interactions between our double-stapled SAH-MPERs and a different anti-MPER Fab that recognizes a helically-structured MPER. We performed a 10E8 competitive ELISA binding assay analogous to that described above for 4E10, and again identified a series of compounds with nanomolar Fab-binding activity, including SAH-MPER$_{(662\text{-}683)}$(A,q), SAH-MPER$_{(662\text{-}683)}$(B,q) and SAH-MPER$_{(662\text{-}683)}$(E,q) (Fig. 7a). Notably, SAH-MPER$_{(662\text{-}683)}$(C,q) and SAH-MPER$_{(662\text{-}683)}$(D,q), which bound to 4E10 Fab in the same nanomolar range as the other constructs (Fig. 6a), showed no binding activity to 10E8 Fab (Fig. 7a). These data are consistent with binding interactions between 10E8 and residues that localize to the N-terminal portion of the MPER epitope[10], such as S668 and L669, which are replaced by stapling amino acids in the (C,q)- and (D,q)-stapled MPER peptides. Although MPER residue W670 also contacts 10E8, replacement of this residue in SAH-MPER$_{(662\text{-}683)}$(E,q) by a staple spanning the W666-W670 positions preserved high affinity 10E8 interaction. Thus, whereas 4E10 Fab sensed no differences in N-terminal staple position due to Fab engagement of the C-terminal portion of the MPER domain only, the 10E8 Fab was more discriminating in the upstream region that included N-terminal residues of the MPER domain.

To determine if hydrocarbon double-stapling maintained the 10E8-bound conformation of the MPER domain, we determined the crystal structure of the 10E8 Fab in complex with SAH-MPER$_{(662\text{-}683KKK)}$(B,q) (Fig. 7b). Crystals of the complex diffracted to 4.15 Å resolution (Table 2), and the structure was solved with molecular replacement and refined to R_{cryst}/R_{free} of 22.1%/27.9%. Two complexes were observed in the asymmetric unit, with their corresponding peptides displaying a Cα root mean square deviation (RMSD) of 0.3 Å across gp41 residues 670-683. Electron density was observed around the C-terminal portion of the peptide, corresponding to gp41 residues S668-K683 for chain P (L669-K683 for chain C), and appeared to only partially cover the staple between residue positions 678 and 681 (Supplementary Fig. 7a). The region upstream of chain P residue S668 (or chain C residue L669) that included the staple between positions 663 and 667 was disordered and could not be built. Nevertheless, the distinctive kink and adjacent N-terminal residues that distinguish 10E8 from 4E10 interactions with the MPER domain are visualized and recapitulated in the 10E8 Fab–SAH-MPER$_{(662\text{-}683KKK)}$(B,q) complex (Fig. 7b).

Overall, the structure revealed that the staple between residue positions 678 and 681 largely reinforced the helical conformation of the C-terminal portion of the MPER peptide, as observed in the structure of 10E8 bound to the native gp41 MPER[10]. The highest degree of structural homology between the 10E8-bound stapled and unmodified peptides was observed between residues 670-683, yielding Cα and all-atom RMSDs of 0.6 and 1.8 Å, respectively (Supplementary Fig. 7b, Supplementary Table 2). Comparison of the contact interfaces between 10E8 and the stapled and unmodified gp41 MPER peptides also revealed a high degree of similarity, with many of the same residues mediating the interactions between them (Supplementary Table 3). An interfacial surface area of 633 Å^2 was buried on the SAH-MPER$_{(662\text{-}683KKK)}$(B,q) peptide, while 713 Å^2 was buried on the antibody. The heavy chain of 10E8 accounted for a majority of the interactions with the double-stapled

peptide, representing 92% of the interface, consistent with the interactions observed between the 10E8 heavy chain and the native gp41 MPER peptide. Interactions between the light chain of 10E8 and the double-stapled peptide also closely mimicked the interactions observed with the native gp41 MPER peptide (Supplementary Table 3). Finally, structural superimposition of the 10E8 Fab–SAH-MPER$_{(662\text{-}683KKK)}$(B,q) and 4E10 Fab–SAH-MPER$_{(671\text{-}683KKK)}$(q) complexes highlights the capacity of hydrocarbon-stapled antigens bearing the 671-683 motif to be differentially engaged by two distinct Fabs, each with potent and broadly neutralizing anti-HIV-1 activity (Fig. 7c)[10,12].

DISCUSSION

The development of a safe and effective HIV-1 vaccine represents one of the most formidable scientific challenges of our time and remains the potential game-changer for curbing the global HIV-1 epidemic. The HIV-1 envelope glycoprotein represents the main target for a humoral immune response, yet the emergence of broadly neutralizing antibodies during natural infection only occurs after one or more years of infection due to a series of viral immune-evasion maneuvers[50–52]. Underlying the many “faces” of the HIV-1 envelope are critical functional intermediates whose structures, although shielded or only transiently exposed, provide a possible blueprint for antigen design. One such motif is the MPER domain, which is the physiologic target for a few broadly neutralizing antibodies. The structures of these antibody-MPER complexes, in addition to their non-neutralizing counterparts, have provided tremendous insight into exactly what three dimensional peptide-encoded configuration may be required to guide an effective anti-HIV-1 immune response[53,54]. How to recapitulate and then stabilize the correct essential structure(s) in order to create a relatively homogeneous candidate immunogen capable of eliciting a safe, broad, and effective immune response has remained elusive.

The helical structure of the MPER domain when bound to distinct broadly neutralizing antibodies, such as 4E10[9] and the recently identified 10E8[10], suggests that structurally constrained peptides may provide a highly desirable template for candidate immunogen design. Seminal work in this area led both to the identification of key residues for 4E10 engagement of a minimal essential helical MPER motif[11] and the demonstration that peptide constraint through the installation of thioether, lactam, or triazole crosslinks, or helix-promoting non-natural amino acids, could reinforce its structure and increase antibody binding affinity[18,33,55]. Structural analysis of the full-length MPER domain in a lipid context revealed a helix-kink-helix conformation, with α-helicity extending to the N-terminus just after a bend induced at F673[17]. We viewed this bipartite structure as an ideal opportunity to increase the immunogenic surface compared to the minimal 4E10 binding epitope (671-683) by reinforcing both helical segments through installation of double constraints. We chose the all-hydrocarbon crosslink afforded by olefin metathesis of installed non-natural amino acids bearing olefin tethers[56] due to the unique proteolytic stability conferred and the protease resistance of the hydrocarbon staple itself[34]. Guided by competitive 4E10 binding activity, we determined that antibody engagement of the C-terminal region of the MPER domain is exquisitely sensitive to the site of staple insertion. Indeed, a single *i, i+3* staple flanking the LW (679-680) sequence, previously shown to be critical for antibody interaction, yielded up to 60-fold enhancement in competitive 4E10

binding activity compared to the unmodified MPER peptide (Fig. 1c, 6a). The 10E8 antibody engages both N- and C-terminal regions of the MPER domain and, in contrast to the 4E10 Fab, 10E8 was sensitive to the positioning of the N-terminal staple. These structure-activity relationship data highlight the capacity of staple scanning to uncover optimal sites for staple incorporation and antigenic structure stabilization.

Our *i, i+3* stapling efforts and the synthetic challenges encountered in generating double-stapled (*i, i+4*), (*i, i+3*) constructs using the traditional S5 non-natural residue, prompted us to develop optimized *i, i+3* stapling chemistry that replaced S5 with R3 at the N-terminal stapling position. This intervention led to facile production of single- and double-stapled MPER peptides incorporating *i, i+3* crosslinks, matching reaction conditions and yields of traditional *i, i+4* stapling with S5 residues. Double-stapled constructs demonstrated nanomolar competitive binding affinity toward 4E10 and 10E8, with the best binder also manifesting 70-fold enhancement in proteolytic stability compared to the corresponding unstapled MPER peptide. This combination of structural stabilization and protease resistance afforded by hydrocarbon double-stapling may represent a highly desirable outcome for candidate immunogen development.

Structural analyses of SAH-MPER peptides in complex with 4E10 and 10E8 Fabs demonstrated the capacity of hydrocarbon stapling to recapitulate native antigenic peptide structures for two distinct broadly neutralizing anti-HIV-1 antibodies, preserving the critical peptide binding interface by positioning the *i, i+3* crosslink on the noninteracting surface. The identification of an incorporated phosphate ion near the antigen-binding region of 4E10 revealed a potential phospholipid binding site. Crystal structures of another broadly neutralizing HIV-1 antibody, 2F5, in complex with the MPER domain identified a putative anionic lipid binding site based on the incorporation of a sulfate ion at the base of the CDR H3 loop at high sulfate concentrations[57]. The binding mode and affinity by which diverse broadly neutralizing antibodies engage the lipid membrane may have important implications for candidate immunogen design and efficacy, and immunologic side effects[38,39,43,57]. By incorporating a phosphate tether into the SAH-MPER design, we effectively accessed the identified phosphate-binding region on 4E10. Indeed, as structured templates, hydrocarbon-stapled peptides are amenable to facile derivatization to incorporate ancillary antibody-binding determinants, and also reinforce unique architectures, such as the helix-kink-helix MPER motif. Thus, hydrocarbon stapling may serve as a useful addition to the arsenal of approaches aimed at fashioning just-the-right peptidic structure to elicit broadly neutralizing antibodies for HIV-1 and perhaps other vaccine targets.

ONLINE METHODS

Peptide Synthesis and Characterization

MPER and SAH-MPER peptides were synthesized, purified, quantified, and subjected to *in vitro* proteolysis testing as previously described[34,58]. Peptides were produced on an Apex 396 (AAPPTEC) automated peptide synthesizer using Rink amide AM LL resin (EMD Biosciences, 0.2 mmol per g resin), at 20 μmol scale. To accomplish single *i, i+3* stapling using S5 residues, prolonged reaction time at elevated temperature (10 h, refluxing dichloroethane) was required to match the yields of traditional *i, i+4* stapling (4h, room

temperature). Protease reaction samples contained 5 μL peptide in DMSO (1 mM stock) and 195 μL of buffer composed of 50 mM Tris-HCl pH 7.4, 2 mM $CaCl_2$, and chymotrypsin (0.5 ng per μL). Chymotryptic peptide fragments were analyzed by liquid chromatography–mass spectrometry (Agilent 1200).

Competitive 4E10 ELISA Binding Assay

A competitive enzyme-linked immunosorbent assay (ELISA) was employed to determine IC_{50}s for SAH-MPER engagement of the 10E8[9] and 4E10[10] antibodies. The following antibodies were obtained through the NIH AIDS Reagent Program, Division of AIDS, NIAID, NIH: HIV-1 gp41 Monoclonal Antibody 4E10 (catalog #10091) from Dr. H. Katinger and HIV-1 anti-gp41 Monoclonal Antibody 10E8 (catalog #12294) from Dr. M. Connors. Microwells were coated overnight at 4°C with 50 μl of 0.1 M $NaHCO_3$ (pH 8.0) containing neutravidin (4 μg per ml). Plates were washed four times using an automated plate washer (Bio-Tek, ELX-50) with phosphate buffered saline containing 0.05% Tween-20 (PBST), and blocked with 4% bovine serum albumin (BSA) in PBST (filled to top of wells) for 45 min at 37 °C. Next, a mixture of biotin-PEG_2-antigen (ELDKWASLWNWFNITNWLWYIK for the 4E10 assay or RRRNEQELLELDKWASLWNWFDITNWLWYIRRRR[10] for the 10E8 assay) (20 nM), 4E10 or 10e8 IgG (0.2 nM), and the competing SAH-MPER peptide (two-fold serial dilution from 1 μM to 1 nM across 10 columns) in PBST with 1% BSA (PBST-BSA), was incubated (125 μL total volume) in a separate 96-well plate at 37°C for 2 h. Controls included wells that lacked SAH-MPER competitor or 4E10 or 10E8 IgG. After washing the blocked neutravidin plate, 100 μL of the binding mixture was added for a 1 hour incubation at 37°C, followed by plate washing and the addition of a 1:5000 dilution of goat anti-human IgG for 10E8 or IgG F(ab′)2 for 4E10 peroxidase conjugate in PBST-BSA. Following incubation at room temperature for 40 min, the wells were washed five times with PBST, and developed by adding 50 μl of tetramethylbenzidine (TMB) solution at room temperature. Wells containing the TMB solution were quenched after approximately 10 minutes by adding 50 μl of H_2SO_4 (2 M), and absorbance at 450 nm was read on a Spectramax microplate reader (Molecular Devices). Experiments were performed in triplicate and repeated at least twice. IC_{50} values for SAH-MPER competition were calculated by nonlinear regression analysis using Prism software (GraphPad).

4E10 Fab Purification and Crystallization of 4E10 Fab–SAH-MPER$_{(671\text{-}683KKK)}$ Complexes

4E10 IgG1(κ) expressed in recombinant Chinese Hamster Ovary cells (CHO) was purchased from Polymun Scientific Immunbiologische Forschung GmbH by the International AIDS Vaccine Initiative (IAVI). The 4E10 antigen-binding fragment Fab was obtained by papain digestion and purified to homogeneity as described previously[12]. The 4E10 Fab concentrated to ~10 mg per ml in 20 mM sodium acetate (pH 5.5) was mixed with the SAH-MPER$_{(671\text{-}683KKK)}$(q) (Ac-NWFNITNZLWXIK-KKK, where Z is R3 and X is S5) in a 1:4 protein:peptide molar ratio and incubated overnight at 4°C prior to setting up crystallizations trials. The IAVI–JCSG–TSRI high-throughput CrystalMation system (Rigaku) was initially used to obtain crystallization conditions for the Fab–SAH-MPER$_{(671\text{-}683KKK)}$(q) complex. Very thin long needles (5–10 μm in diameter) appeared in 2–3 weeks in drops containing 4E10 Fab–SAH-MPER$_{(671\text{-}683KKK)}$(q) and reservoir solution (50:50) equilibrated against

0.2 M sodium chloride, 0.1 M Na–K phosphate pH 6.2, and 50% polyethylene glycol 200. Micro and macro-seeding techniques using the reservoir solution were used to improve crystal size. The crystals were cryoprotected in mother liquor solutions containing ~60% polyethylene glycol 200.

The 4E10 Fab stock mixed with SAH-MPER$_{(671\text{-}683KKK)}$(q)pSer (Ac-NWFNITNZLWXI*KKK, where Z is R3, X is S5 and * is Dab-Gly-pSer) in a 1:5 molar ratio was incubated overnight at 4°C for complex formation. The initial screening trials lead to identification of several crystallization conditions that produced extremely small crystals. One of the conditions lacking PO_4 ions was then used for further crystal optimization. Briefly, tiny needles crystals, grown by mixing equal amounts of 4E10 Fab–SAH-MPER$_{(671\text{-}683KKK)}$(q)pSer with reservoir solution (20% PEG 2,000, 0.1M Tris pH 7.0), were crushed using a Hampton Seeding bead and then seeded into a JCSG Top 96 screen (http://www.jcsg.org/top96). Long (*ca.* 200–300 μm), thick (*ca.* 60–70 μm) needle-like crystals grew from a mixture of equal amounts of complex and reservoir solution (0.2 M $MgCl_2$, 0.1M MES pH 5.5, 40% PEG 400) and 20% of the aforementioned seeding stock in the final drop. The crystals were cryoprotected prior to data collection in mother liquor solution containing about 46% PEG 400.

4E10 Data collection, Structure Determination and Refinement

The X-ray diffraction data for 4E10 Fab–SAH-MPER$_{(671\text{-}683KKK)}$(q) were collected at 110 K on a MARMosaic 300 detector using synchrotron radiation (λ = 1.03317 Å) at the Advanced Photon Source (APS) 23ID-D beam line from crystals of ~40 μm in diameter that diffracted to approximately 2.9 Å resolution. To increase completeness in the high-resolution shell, X-ray data sets from two crystals were indexed and scaled together using HKL2000[59]. The diffraction data were indexed in space group $P6_122$ as suggested by pointless[60], xprep[61] and phenix-Xtriage[62] programs. Molecular replacement was performed with Phaser[63], which led to one Fab–peptide complex per asymmetric unit with a rotation and translation function Z-scores of 10.6 and 42.8, respectively, and a log-likelihood gain of 3,655. The initial positions of the models were optimized by rigid body refinement using Phenix[64]. Rebuilding of the model was performed in Coot[65]. Refinement was accomplished with Phenix using secondary structure restraints coupled with the refinement of individual atomic coordinates using gradient-driven (LBFGS) minimization and torsion angle simulated annealing, occupancy refinement, refinement of individual atomic displacement parameters and TLS refinement. Optimization of X-ray–stereochemistry and X-ray–ADP weights were also performed during refinement cycles. X-ray data quality and refinement statistics are included in Table 1. The Ramachandran statistics show 90.2% of the residues in the most favored regions, 5.8% in the additional allowed regions, and 4.0% in the disallowed regions. PyMOL (http://www.pymol.org/) was used to generate the crystallographic images.

The 4E10 Fab–SAH-MPER$_{(671\text{-}683KKK)}$(q)pSer structure was solved from a single crystal X-ray diffraction data set (2.68 Å resolution) collected at 110 K on a MARMosaic 300 detector at the APS 23ID-B beam line using a radiation wavelength of 1.03330 Å. Although the crystals were obtained from a different mother liquor composition than that of the 4E10

Fab–SAH-MPER$_{(671\text{-}683KKK)}$(q) crystals, the auto-indexing suggested the same $P6_122$ space group with similar unit cell values (Table 1). Molecular replacement performed using Phaser[63] with only the Fab residues of the 4E10 Fab–SAH-MPER$_{(671\text{-}683KKK)}$(q) complex resulted in one complex per asymmetric unit with a model rotation and translation function Z-scores of 13.3 and 68.2, respectively, and a log-likelihood gain of 4,403. Model building and refinement was performed as for the 4E10 Fab–SAH-MPER$_{(671\text{-}68KKK)}$(q) complex except that cartesian-simulated annealing was used instead. The Ramachandran statistics show 93.8% of the residues in the most favored regions, 4.7% in the additional allowed regions, and 1.5% in the disallowed regions.

Expression and Purification of 10E8 and Generation of Fabs

Transient expression of the 10E8 antibody was undertaken in 293F cells or 293 Expi cells per the manufacturer's instructions (Life Technologies) by co-transfection of equal amounts of the 10E8 heavy and light chain plasmids, as previously described[66]. 10E8 IgG was purified by capture with Protein A sepharose (Pierce) followed by elution in low pH (Pierce) with adjustment of eluate pH with Tris-Cl pH 8.0. The 10E8 Fab was prepared using endoproteinase Lys-C (Roche) digestion, as described[66]. The LysC protease was added at concentrations of 1:1,000 to 1:10,000 and the digestion undertaken at 37°C for 4–6 h. Digestion reactions were stopped with protease inhibitor tablets (Roche) and cleaved products were run over a Protein A column to segregate the Fc fragment. 10E8 Fab was then subjected to cation exchange (Mono S) and size-exclusion (S200) chromatography, followed by dialysis of peak fractions into 150 mM NaCl, 2.5 mM Tris, pH 7.5, 0.02% NaN_3.

10E8 Crystallization, Structure Determination, and Structural Analysis

Purified 10E8 Fab in complex with SAH-MPER$_{(662\text{-}683KKK)}$(B,q) was set up in crystallization screens using a Honeybee 963 robot. 576 initial conditions adapted from the commercially available Hampton (Hampton Research), Precipitant Synergy (Emerald Biosystems), and Wizard (Emerald Biosystems) crystallization screens were utilized to set up vapor diffusion sitting drop crystallizations at 20°C. Crystal trays were imaged with the use of a Rockimager (Formulatrix) and crystal hits were optimized manually. Crystals of the 10E8 Fab in complex with SAH-MPER$_{(662\text{-}683KKK)}$(B,q) were obtained in a crystallization condition comprised of 32% Isopropanol, 7.5% PEG 8000, 0.1 M Imidazole pH 6.5. Diffraction to 4.15 Å resolution was obtained in a cryoprotectant composed of mother liquor supplemented with 50% sucrose and excess peptide. Diffraction data were collected at SER CAT ID-22 beamline of the Advanced Photon Source (Argonne, IL) using a radiation wavelength of 1.0000 Å and processed using HKL-2000[59]. The structure was solved with molecular replacement using Phaser[63], with the high resolution structure of 10E8 Fab in complex with gp41 MPER peptide (PDB ID 4G6F) serving as the search model. Refinement was undertaken with Phenix[67], utilizing PDB ID 4G6F as a reference model, with iterative model building in Coot[68]. Structures were validated with MolProbity[69], and then analyzed using PISA for buried surface areas and residues[70], and lsqkab for RMSD alignments (ccp4 Package)[71]. The Ramachandran statistics show 96.56% of the residues in the most favored regions, 2.77% in the additional allowed regions, and 0.67% in the disallowed regions.

Supplementary Material

Refer to Web version on PubMed Central for supplementary material.

Acknowledgments

We thank E. Smith for graphics assistance, D. Ekiert and E. Reinherz for insightful discussions, M. Connors (National Institute of Allergy and Infectious Diseases) for his generosity in providing us with a sample of 10E8 antibody, and Y. Yang and P. Acharya for technical support. We are grateful to the National Institutes of Health (NIH) AIDS Reagent Program for providing us with 4E10 and 10E8 antibodies. This work was supported by the U.S. NIH Grant 1R01 AI084102 (L.D.W.), R01 AI36082 (I.A.W.), Scripps Center for HIV/AIDS Vaccine Immunology and Immunogen Discovery (CHAVI-ID) UM1 AI100663 (I.A.W.), the International AIDS Vaccine Initiative (IAVI), Neutralizing Antibody Center, IAVI Collaboration for AIDS Vaccine Discovery, the Bill and Melinda Gates Foundation, and the Intramural Research Program of the Vaccine Research Center, National Institute of Allergy and Infectious Diseases (NIAID), NIH. Use of the 23-ID sector at Advanced Photon Source was supported by the U. S. Department of Energy, Office of Science, Office of Basic Energy Sciences, under Contract No. DE-AC02-06CH11357.

References

1. Fauci AS, et al. HIV vaccine research: the way forward. Science. 2008; 321:530–2. [PubMed: 18653883]
2. Rits-Volloch S, Frey G, Harrison SC, Chen B. Restraining the conformation of HIV-1 gp120 by removing a flexible loop. Embo J. 2006; 25:5026–35. [PubMed: 17006538]
3. Matthews TJ, et al. Interaction between the human T-cell lymphotropic virus type IIIB envelope glycoprotein gp120 and the surface antigen CD4: role of carbohydrate in binding and cell fusion. Proc Natl Acad Sci U S A. 1987; 84:5424–8. [PubMed: 3037551]
4. Xiao L, et al. CCR5 coreceptor usage of non-syncytium-inducing primary HIV-1 is independent of phylogenetically distinct global HIV-1 isolates: delineation of consensus motif in the V3 domain that predicts CCR-5 usage. Virology. 1998; 240:83–92. [PubMed: 9448692]
5. Buzon V, et al. Crystal structure of HIV-1 gp41 including both fusion peptide and membrane proximal external regions. PLoS Pathog. 2010; 6:e1000880. [PubMed: 20463810]
6. Chan DC, Fass D, Berger JM, Kim PS. Core structure of gp41 from the HIV envelope glycoprotein. Cell. 1997; 89:263–73. [PubMed: 9108481]
7. Muster T, et al. A conserved neutralizing epitope on gp41 of human immunodeficiency virus type 1. J Virol. 1993; 67:6642–7. [PubMed: 7692082]
8. Zwick MB, et al. Broadly neutralizing antibodies targeted to the membrane-proximal external region of human immunodeficiency virus type 1 glycoprotein gp41. J Virol. 2001; 75:10892–10905. [PubMed: 11602729]
9. Stiegler G, et al. A potent cross-clade neutralizing human monoclonal antibody against a novel epitope on gp41 of human immunodeficiency virus type 1. AIDS Res Hum Retroviruses. 2001; 17:1757–1765. [PubMed: 11788027]
10. Huang J, et al. Broad and potent neutralization of HIV-1 by a gp41-specific human antibody. Nature. 2012; 491:406–12. [PubMed: 23151583]
11. Brunel FM, et al. Structure-function analysis of the epitope for 4E10, a broadly neutralizing human immunodeficiency virus type 1 antibody. J Virol. 2006; 80:1680–7. [PubMed: 16439525]
12. Cardoso RM, et al. Broadly neutralizing anti-HIV antibody 4E10 recognizes a helical conformation of a highly conserved fusion-associated motif in gp41. Immunity. 2005; 22:163–73. [PubMed: 15723805]
13. Coutant J, et al. Both lipid environment and pH are critical for determining physiological solution structure of 3-D-conserved epitopes of the HIV-1 gp41-MPER peptide P1. Faseb J. 2008; 22:4338–51. [PubMed: 18776068]
14. Huarte N, Lorizate M, Kunert R, Nieva JL. Lipid modulation of membrane-bound epitope recognition and blocking by HIV-1 neutralizing antibodies. FEBS Lett. 2008; 582:3798–804. [PubMed: 18930052]

15. Montero M, van Houten NE, Wang X, Scott JK. The membrane-proximal external region of the human immunodeficiency virus type 1 envelope: dominant site of antibody neutralization and target for vaccine design. Microbiol Mol Biol Rev. 2008; 72:54–84. [PubMed: 18322034]
16. Ofek G, et al. Structure and mechanistic analysis of the anti-human immunodeficiency virus type 1 antibody 2F5 in complex with its gp41 epitope. J Virol. 2004; 78:10724–37. [PubMed: 15367639]
17. Sun ZY, et al. HIV-1 broadly neutralizing antibody extracts its epitope from a kinked gp41 ectodomain region on the viral membrane. Immunity. 2008; 28:52–63. [PubMed: 18191596]
18. Cardoso RM, et al. Structural basis of enhanced binding of extended and helically constrained peptide epitopes of the broadly neutralizing HIV-1 antibody 4E10. J Mol Biol. 2007; 365:1533–44. [PubMed: 17125793]
19. Penn-Nicholson A, et al. Assessment of antibody responses against gp41 in HIV-1-infected patients using soluble gp41 fusion proteins and peptides derived from M group consensus envelope. Virology. 2008; 372:442–56. [PubMed: 18068750]
20. Scherer EM, Leaman DP, Zwick MB, McMichael AJ, Burton DR. Aromatic residues at the edge of the antibody combining site facilitate viral glycoprotein recognition through membrane interactions. Proc Natl Acad Sci U S A. 2010; 107:1529–34. [PubMed: 20080706]
21. Ofek G, et al. Elicitation of structure-specific antibodies by epitope scaffolds. Proc Natl Acad Sci U S A. 2010; 107:17880–7. [PubMed: 20876137]
22. Guenaga J, et al. Heterologous epitope-scaffold prime:boosting immuno-focuses B cell responses to the HIV-1 gp41 2F5 neutralization determinant. PLoS One. 2011; 6:e16074. [PubMed: 21297864]
23. Correia BE, et al. Computational design of epitope-scaffolds allows induction of antibodies specific for a poorly immunogenic HIV vaccine epitope. Structure. 2010; 18:1116–26. [PubMed: 20826338]
24. Correia BE, et al. Computational protein design using flexible backbone remodeling and resurfacing: case studies in structure-based antigen design. J Mol Biol. 2011; 405:284–97. [PubMed: 20969873]
25. Stanfield RL, et al. Structure-based design of a protein immunogen that displays an HIV-1 gp41 neutralizing epitope. J Mol Biol. 2011; 414:460–76. [PubMed: 22033480]
26. Yi G, et al. Chimeric rhinoviruses displaying MPER epitopes elicit anti-HIV neutralizing responses. PLoS One. 2013; 8:e72205. [PubMed: 24039745]
27. Dawood R, et al. Generation of HIV-1 potent and broad neutralizing antibodies by immunization with postfusion HR1/HR2 complex. Aids. 2013; 27:717–30. [PubMed: 23719346]
28. Wahome N, et al. Conformation-specific display of 4E10 and 2F5 epitopes on self-assembling protein nanoparticles as a potential HIV vaccine. Chem Biol Drug Des. 2012; 80:349–57. [PubMed: 22650354]
29. Black M, Trent A, Tirrell M, Olive C. Advances in the design and delivery of peptide subunit vaccines with a focus on toll-like receptor agonists. Expert Rev Vaccines. 2010; 9:157–73. [PubMed: 20109027]
30. Purcell AW, McCluskey J, Rossjohn J. More than one reason to rethink the use of peptides in vaccine design. Nat Rev Drug Discov. 2007; 6:404–14. [PubMed: 17473845]
31. Slingluff CL Jr. The present and future of peptide vaccines for cancer: single or multiple long or short alone or in combination? Cancer J. 2011; 17:343–50. [PubMed: 21952285]
32. Ho J, et al. Conformational constraints imposed on a pan-neutralizing HIV-1 antibody epitope result in increased antigenicity but not neutralizing response. Vaccine. 2005; 23:1559–73. [PubMed: 15694508]
33. Ingale S, Gach JS, Zwick MB, Dawson PE. Synthesis and analysis of the membrane proximal external region epitopes of HIV-1. J Pept Sci. 2010; 16:716–22. [PubMed: 21104968]
34. Bird GH, et al. Hydrocarbon double-stapling remedies the proteolytic instability of a lengthy peptide therapeutic. Proc Natl Acad Sci U S A. 2010; 107:14093–14098. [PubMed: 20660316]
35. Leaman DP, Zwick MB. Increased functional stability and homogeneity of viral envelope spikes through directed evolution. PLoS Pathog. 2013; 9:e1003184. [PubMed: 23468626]
36. Zolla-Pazner S. A critical question for HIV vaccine development: which antibodies to induce? Science. 2014; 345:167–8. [PubMed: 25013066]

37. Scherer EM, Zwick MB, Teyton L, Burton DR. Difficulties in eliciting broadly neutralizing anti-HIV antibodies are not explained by cardiolipin autoreactivity. Aids. 2007; 21:2131–2139. [PubMed: 18090039]
38. Matyas GR, et al. Neutralizing antibodies induced by liposomal HIV-1 glycoprotein 41 peptide simultaneously bind to both the 2F5 or 4E10 epitope and lipid epitopes. Aids. 2009; 23:2069–2077. [PubMed: 19710597]
39. Matyas GR, Beck Z, Karasawas N, Alving CR. Lipid binding properties of 4E10, 2175, and WR304 monoclonal antibodies that neutralize HIV-1. Biochim Biophys Acta. 2009; 1788:660–665. [PubMed: 19100711]
40. Maeso R, et al. Interaction of Anti-HIV Type 1 Antibody 2F5 with Phospholipid Bilayers and Its Relevance for the Mechanism of Virus Neutralization. AIDS Res Hum Retroviruses. 2011; 27:863–876. [PubMed: 21142698]
41. Haynes BF, et al. Cardiolipin polyspecific autoreactivity in two broadly neutralizing HIV-1 antibodies. Science. 2005; 308:1906–8. [PubMed: 15860590]
42. Alam SM, et al. The role of antibody polyspecificity and lipid reactivity in binding of broadly neutralizing anti-HIV-1 envelope human monoclonal antibodies 2F5 and 4E10 to glycoprotein 41 membrane proximal envelope epitopes. J Immunol. 2007; 178:4424–35. [PubMed: 17372000]
43. Chen J, et al. Mechanism of HIV-1 Neutralization by Antibodies Targeting a Membrane-Proximal Region of gp41. J Virol. 2014; 88:1249–58. [PubMed: 24227838]
44. Bernal F, et al. A stapled p53 helix overcomes HDMX-mediated suppression of p53. Cancer Cell. 2010; 18:411–22. [PubMed: 21075307]
45. LaBelle JL, et al. A stapled BIM peptide overcomes apoptotic resistance in hematologic cancers. J Clin Invest. 2012; 122:2018–31. [PubMed: 22622039]
46. Takada K, et al. Targeted disruption of the BCL9/beta-catenin complex inhibits oncogenic Wnt signaling. Sci Transl Med. 2012; 4:148ra117.
47. Walensky LD, et al. Activation of apoptosis in vivo by a hydrocarbon-stapled BH3 helix. Science. 2004; 305:1466–70. [PubMed: 15353804]
48. Kim YW, Kutchukian PS, Verdine GL. Introduction of all-hydrocarbon i,i+3 staples into alpha-helices via ring-closing olefin metathesis. Org Lett. 2010; 12:3046–9. [PubMed: 20527740]
49. Finton KA, et al. Autoreactivity and exceptional CDR plasticity (but not unusual polyspecificity) hinder elicitation of the anti-HIV antibody 4E10. PLoS Pathog. 2013; 9:e1003639. [PubMed: 24086134]
50. Hraber P, et al. Prevalence of broadly neutralizing antibody responses during chronic HIV-1 infection. Aids. 2014; 28:163–9. [PubMed: 24361678]
51. Liao HX, et al. Co-evolution of a broadly neutralizing HIV-1 antibody and founder virus. Nature. 2013; 496:469–76. [PubMed: 23552890]
52. Locci M, et al. Human circulating PD-(+)1CXCR3(−)CXCR5(+) memory Tfh cells are highly functional and correlate with broadly neutralizing HIV antibody responses. Immunity. 2013; 39:758–69. [PubMed: 24035365]
53. Frey G, et al. Distinct conformational states of HIV-1 gp41 are recognized by neutralizing and non-neutralizing antibodies. Nat Struct Mol Biol. 2010; 17:1486–91. [PubMed: 21076402]
54. Frey G, et al. A fusion-intermediate state of HIV-1 gp41 targeted by broadly neutralizing antibodies. Proc Natl Acad Sci U S A. 2008; 105:3739–44. [PubMed: 18322015]
55. Ingale S, Dawson PE. On resin side-chain cyclization of complex peptides using CuAAC. Org Lett. 2011; 13:2822–5. [PubMed: 21553819]
56. Schafmeister C, Po J, Verdine G. An all-hydrocarbon cross-linking system for enhancing the helicity and metabolic stability of peptides. J Am Chem Soc. 2000; 122:5891–5892.
57. Julien JP, Bryson S, Nieva JL, Pai EF. Structural details of HIV-1 recognition by the broadly neutralizing monoclonal antibody 2F5: epitope conformation, antigen-recognition loop mobility, and anion-binding site. J Mol Biol. 2008; 384:377–92. [PubMed: 18824005]
58. Bird GH, Bernal F, Pitter K, Walensky LD. Synthesis and biophysical characterization of stabilized alpha-helices of BCL-2 domains. Methods Enzymol. 2008; 446:369–86. [PubMed: 18603134]

59. Otwinowski Z, Minor W. Processing of X-ray diffraction data collected in oscillation mode. Macromol Crystallogr A. 1997; 276:307–326.
60. Evans P. Scaling and assessment of data quality. Acta Crystallogr D Biol Crystallogr. 2006; 62:72–82. [PubMed: 16369096]
61. Sheldrick GM. A short history of SHELX. Acta Crystallogr A. 2008; 64:112–122. [PubMed: 18156677]
62. Zwart PH, Grosse-Kunsteleve RW, Adams PD. Characterization of X-ray data sets. CCP4 Newsletter. 2005; 42:1–10.
63. McCoy AJ, et al. Phaser crystallographic software. J Appl Crystallogr. 2007; 40:658–674. [PubMed: 19461840]
64. Adams PD, et al. PHENIX: a comprehensive Python-based system for macromolecular structure solution. Acta Crystallogr D Biol Crystallogr. 2010; 66:213–221. [PubMed: 20124702]
65. Emsley P, Lohkamp B, Scott WG, Cowtan K. Features and development of Coot. Acta Crystallogr D Biol Crystallogr. 2010; 66:486–501. [PubMed: 20383002]
66. Huang J, et al. Broad and potent neutralization of HIV-1 by a gp41-specific human antibody. Nature. 2012; 491:406–412. [PubMed: 23151583]
67. Adams PD, et al. PHENIX: building new software for automated crystallographic structure determination. Acta Crystallogr D Biol Crystallogr. 2002; 58:1948–1954. [PubMed: 12393927]
68. Emsley P, Cowtan K. Coot: model-building tools for molecular graphics. Acta Crystallogr D Biol Crystallogr. 2004; 60:2126–2132. [PubMed: 15572765]
69. Davis IW, et al. MolProbity: all-atom contacts and structure validation for proteins and nucleic acids. Nucleic Acids Res. 2007; 35:W375–W383. [PubMed: 17452350]
70. Krissinel E, Henrick K. Inference of macromolecular assemblies from crystalline state. J Mol Biol. 2007; 372:774–797. [PubMed: 17681537]
71. Winn MD, et al. Overview of the CCP4 suite and current developments. Acta Crystallogr D Biol Crystallogr. 2011; 67:235–42. [PubMed: 21460441]

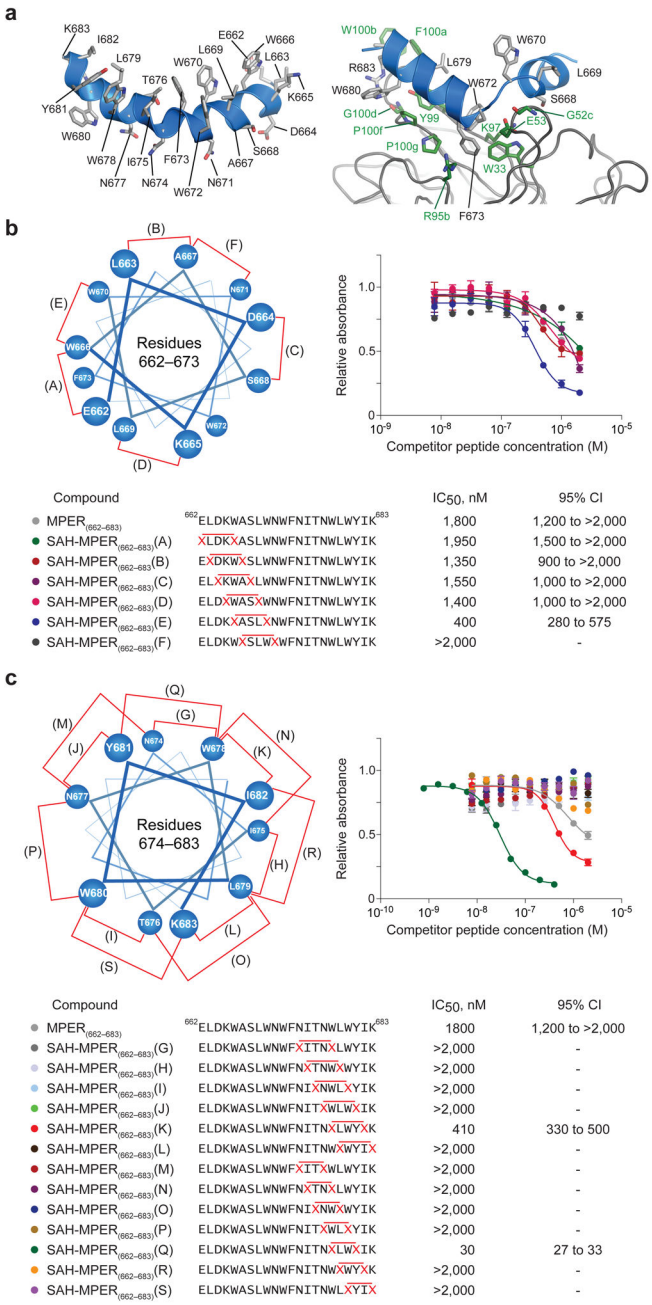

Figure 1. Design and 4E10 Binding Activity of Hydrocarbon-Stapled MPER Peptides

(a) Structure of the extended HIV-1 MPER domain in the lipid environment[17] (left) and when bound to the broadly neutralizing 10E8 antibody (4G6F)[10] (right). (b) Single *i*, *i+4* hydrocarbon staples were sequentially inserted into the N-terminal half of the MPER sequence and the resultant SAH-MPER$_{(662-683)}$ constructs (A–F) subjected to competitive 4E10 ELISA assay. The N-terminal helical wheel depicts staple placement along the MPER sequence. (c) Single *i*, *i+4* and *i*, *i+3* hydrocarbon staples were sequentially inserted into the C-terminal half of the MPER sequence and the binding activity of the resultant SAH-MPER$_{(662-683)}$ constructs (G–S) evaluated by competitive 4E10 ELISA assay. The C-

terminal helical wheel depicts staple placement along the MPER sequence. Error bars, s.e.m. (n = 3 binding assay replicates).

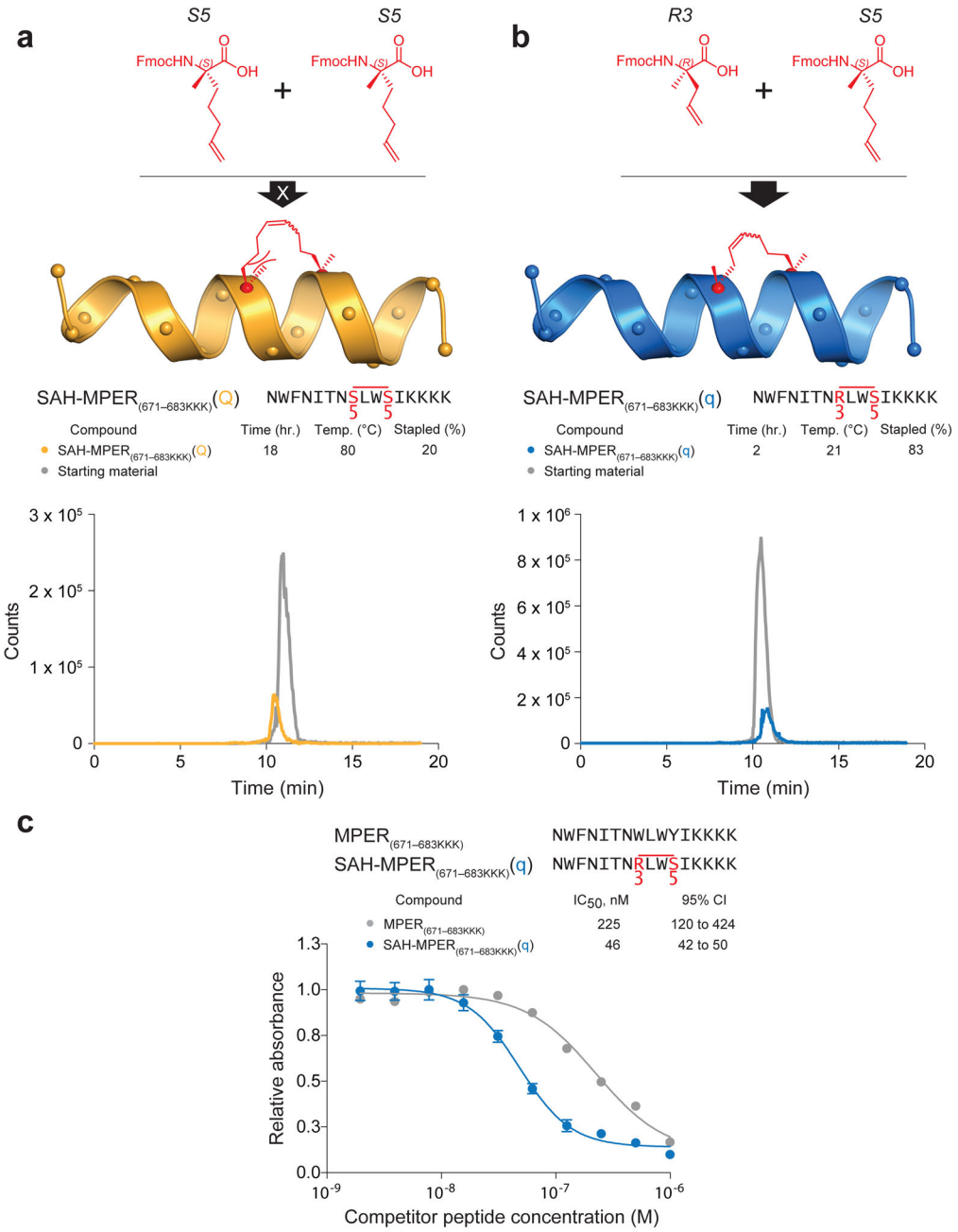

Figure 2. Chemical Optimization of *i, i+3* Hydrocarbon Stapling

(a) Design and synthesis of SAH-MPER$_{(671\text{-}683KKK)}$(Q) using S5 olefinic tethers to generate the *i*, *i+3* staple. HPLC traces of starting material (grey) and product (yellow) demonstrate the low yield of reaction product even after prolonged incubation at reflux conditions. (b) Design and synthesis of SAH-MPER$_{(671\text{-}683KKK)}$(q), in which the N-terminal S5 residue was replaced with R3, leading to efficient *i*, *i+3* olefin metathesis using standard reaction conditions. HPLC traces of starting material (grey) and product (blue) demonstrate the high yield of reaction product. (c) Competitive 4E10 binding activity of SAH-

$MPER_{(671\text{-}683KKK)}$(q) compared to the corresponding unstapled peptide. Error bars, s.e.m. (*n* = 3 binding assay replicates). Fmoc, Fluorenylmethoxycarbonyl

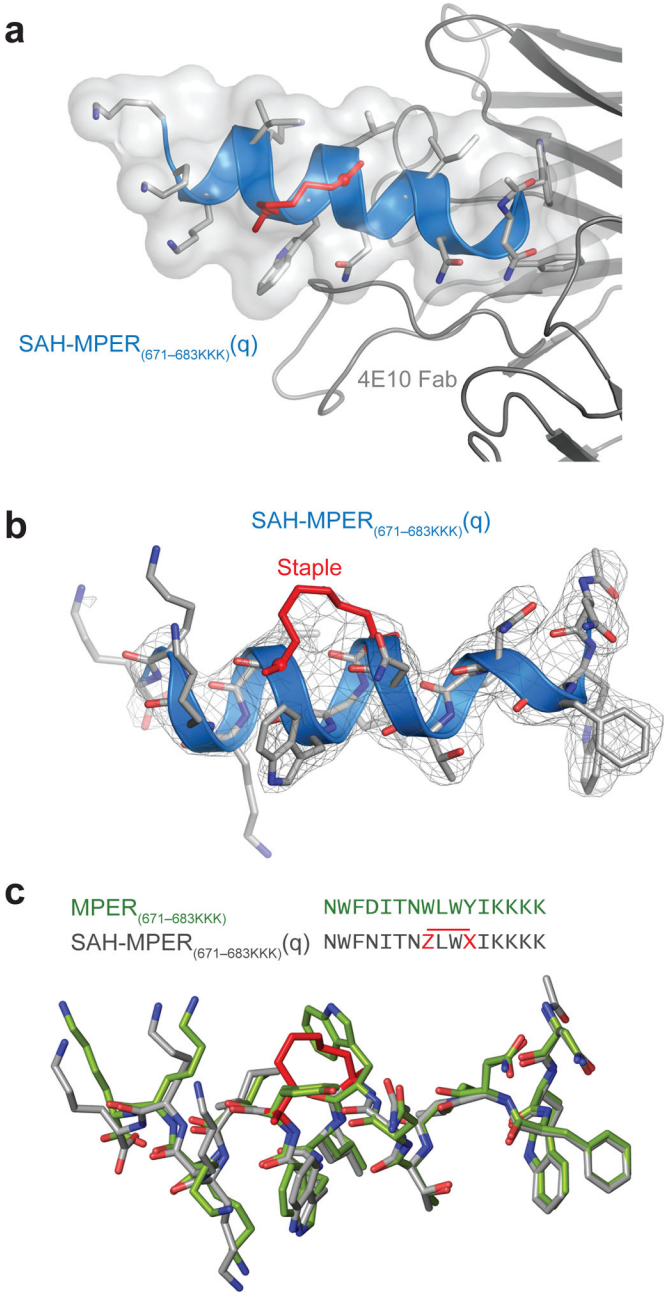

Figure 3. Structural Analysis of the 4E10 Fab–SAH-MPER$_{(671\text{-}683KKK)}$(q) Complex

(a) Crystal structure of SAH-MPER$_{(671\text{-}683KKK)}$(q) (shown as a blue ribbon and gray transparent van der Waals surface) bound to 4E10 Fab at 2.9 Å resolution. (b) 2Fo-Fc electron density map (1σ level) of the antibody-bound SAH-MPER$_{(671\text{-}683KKK)}$(q) peptide. (c) Superimposition of the native (green, 2FX7)[18] and *i*, *i+3*-stapled (gray) MPER$_{(671\text{-}683KKK)}$ peptides highlights the similarity of antibody-bound structures, aside from the appended C-terminal lysines and the incorporated staple. Z and X represent R3 and S5, respectively.

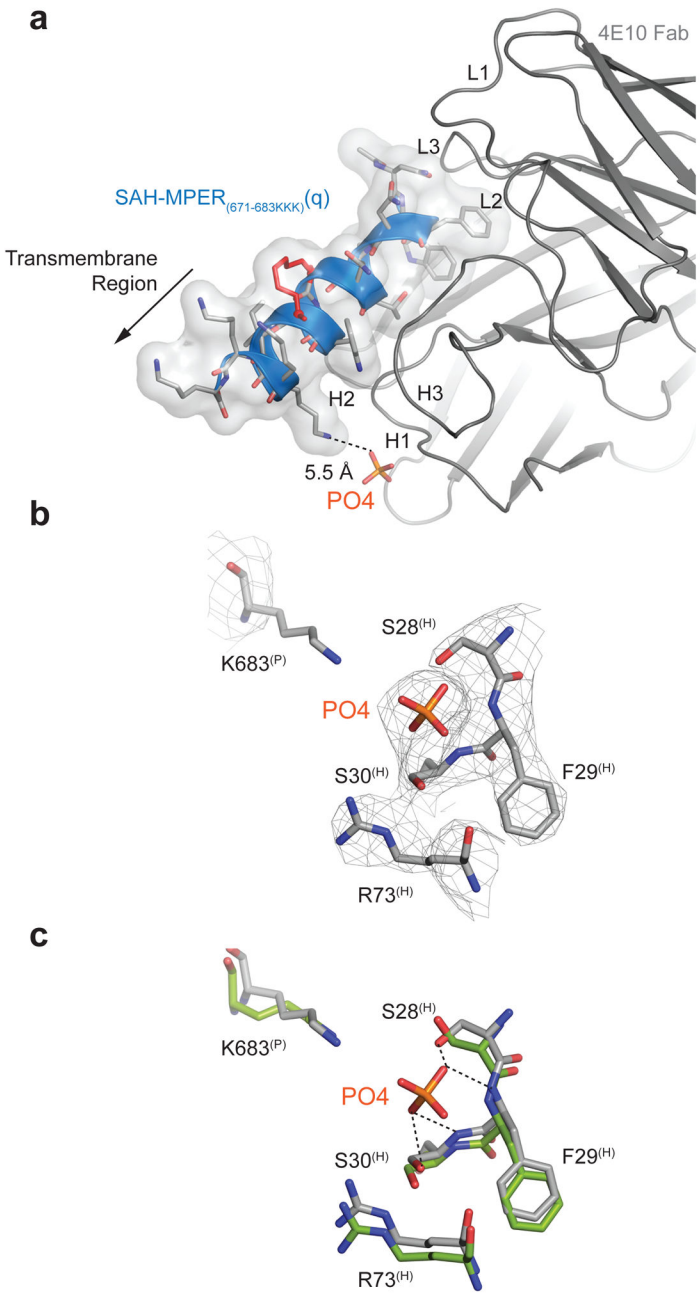

Figure 4. Identification of a Candidate Phospholipid Binding Site at the 4E10 Interface

(a) Incorporation of a phosphate ion from the mother liquor into the crystal structure of the 4E10 Fab–SAH-MPER$_{(671\text{-}683KKK)}$(q) complex. The presence of a phosphate binding site in the CDR-H1 loop region of 4E10 is consistent with its binding mode at the membrane surface. The transmembrane region (replaced here by three lysines for solubility purposes) that would be membrane embedded in the virion is indicated with an arrow. (b) 2Fo-Fc electron density map (1σ level) of the phosphate binding site located between residues S28$^{(H)}$ and S30$^{(H)}$ of the CDR-H1 loop. (c) Superimposition of the phosphate-incorporated

site of the 4E10 Fab–SAH-MPER$_{(671\text{-}683KKK)}$(q) structure (gray) with that region of the 4E10 Fab–native MPER$_{(671\text{-}683KKK)}$ peptide complex (green; PDB entry 2FX7[18]).

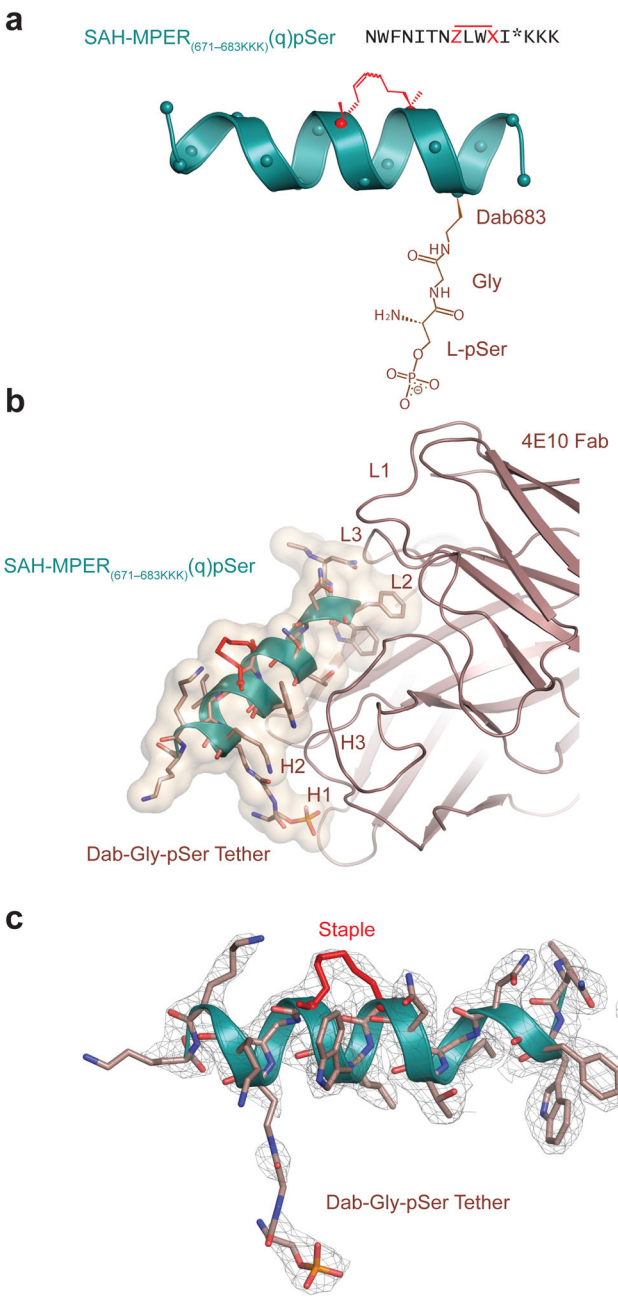

Figure 5. A Phosphate Tether Incorporated into SAH-MPER$_{(671\text{-}683KKK)}$(q) Engages the Putative Lipid Binding Site

(a) Position 683 of SAH-MPER$_{(671\text{-}683KKK)}$(q) was derivatized with a Dab-Gly-pSer tether (brown) to span the measured 5.5 Å between the primary amine of Lys683 and the phosphate observed at the 4E10 Fab–SAH-MPER$_{(671\text{-}683KKK)}$(q) interface. (b) Crystal structure of the SAH-MPER$_{(671\text{-}683KKK)}$(q)pSer complex (shown as a green ribbon and wheat transparent Van der Waals surface) bound to 4E10 at 2.68 Å resolution. (c) The 2Fo-Fc electron density map (1σ level) of the antibody-bound SAH-MPER$_{(671\text{-}683KKK)}$(q)pSer construct.

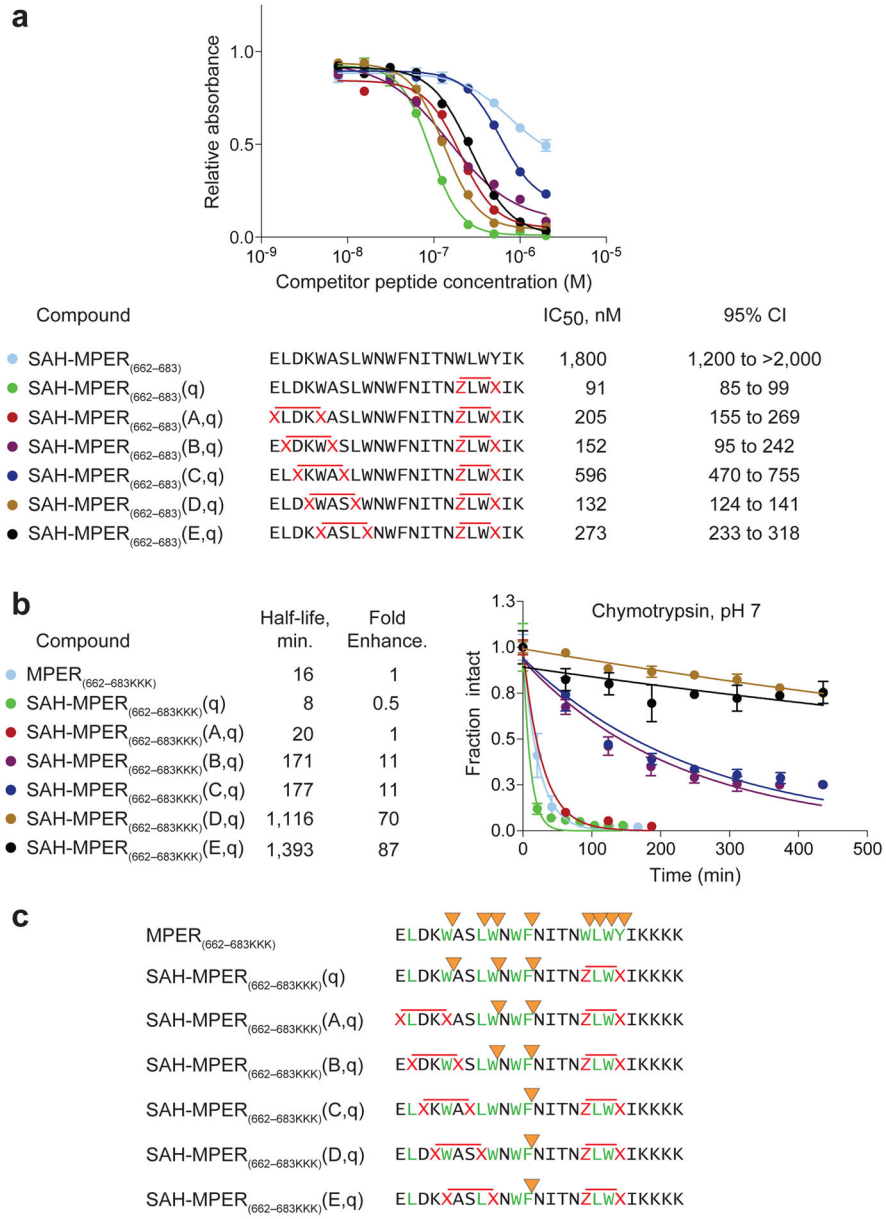

Figure 6. Synthesis, Protease Stability, and 4E10 Binding Activity of Double-stapled SAH-MPER Peptides

(a) A series of double-stapled SAH-MPER$_{(662-683)}$ peptides were tested for 4E10 binding activity by competitive ELISA assay. (b) Comparative chymotrypsin resistance of SAH-MPER$_{(662-683)}$ peptides, as monitored by LC/MS over time. Proteolysis was performed with SAH-MPER constructs bearing C-terminal KKKs to optimize peptide ionization for MS analysis. Error bars, s.e.m. (n = 3 proteolysis reaction replicates). (c) MS-based peptide fragment analysis identified the sites of chymotrypsin proteolysis. Whereas chymotrypsin sites (yellow arrowheads) located within or adjacent to the installed staples (red X-X, Z-X pairs) were completely protected from proteolysis, the cleavage kinetics for intervening site(s) was progressively slowed (A,q<B,q<C,q<D,q<E,q) by the induced structure of the approaching N-terminal staple (red X-X pairs).

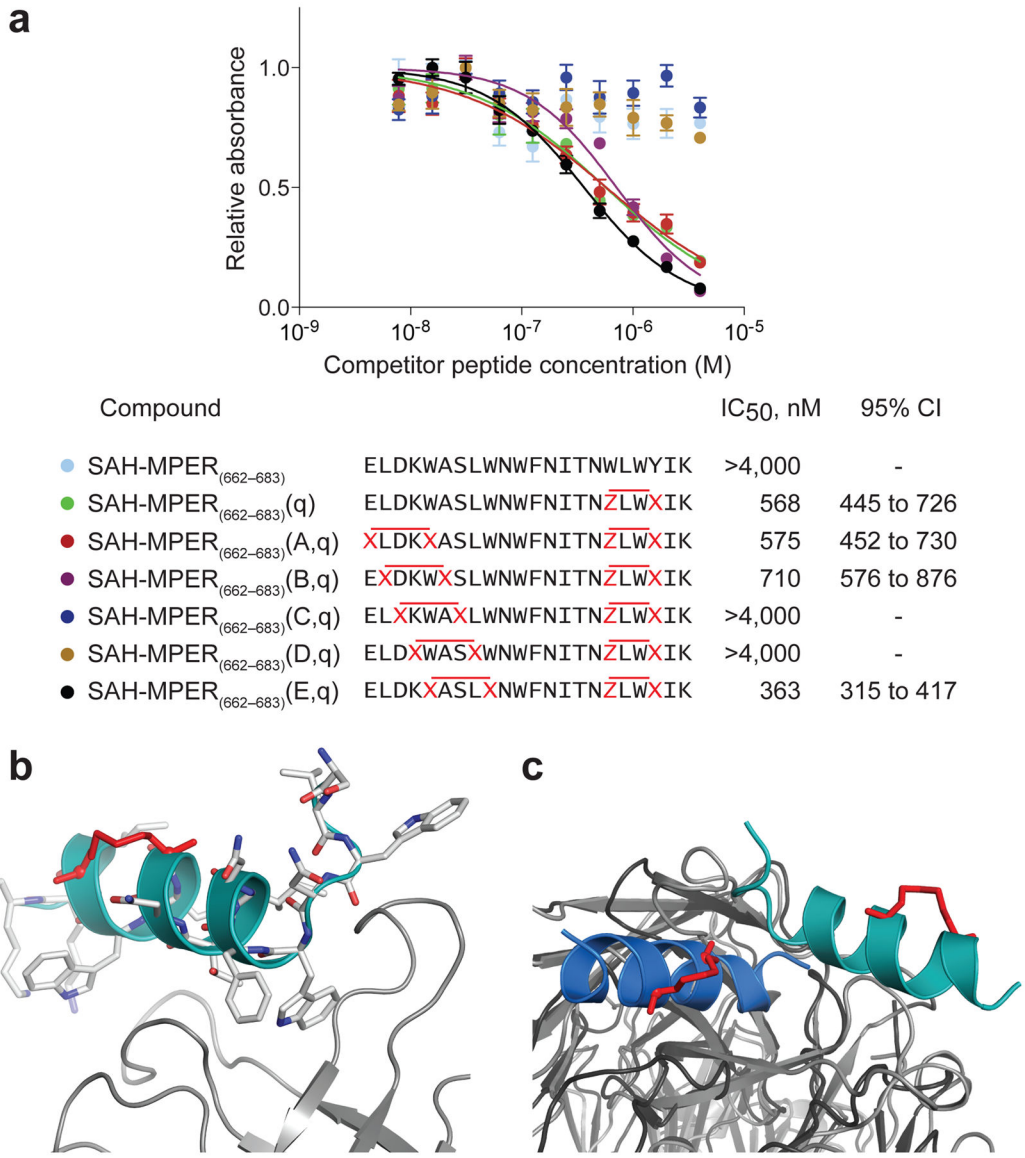

Figure 7. 10E8 Binding Activity of Double-stapled SAH-MPER Peptides and Structural Analysis of the 10E8 Fab–SAH-MPER$_{(662\text{-}683KKK)}$(B,q) Complex

(a) Comparative binding activity of double-stapled SAH-MPER$_{(662\text{-}683)}$ peptides for 10E8, as measured by competitive ELISA assay against the unmodified 10E8 ligand RRRNEQELLELDKWASLWNWFDITNWLWYIRRRR[10]. (b) Crystal structure of SAH-MPER$_{(662\text{-}683KKK)}$(B,q) (shown as a cyan ribbon with stick residues) bound to 10E8 Fab at 4.15 Å resolution. (c) Superimposition of the 4E10 Fab–SAH-MPER$_{(671\text{-}683KKK)}$(q) and 10E8 Fab–SAH-MPER$_{(662\text{-}683KKK)}$(B,q) complexes highlights how the two anti-HIV Fabs differentially engage the stapled MPER antigens.

Table 1

Data collection and refinement statistics for the 4E10 Fab–SAH-MPER$_{(671\text{-}683KKK)}$(q) and the 4E10 Fab–SAH-MPER$_{(671\text{-}683KKK)}$(q)pSer complexes

	4E10 Fab SAH-MPER$_{(671\text{-}683KKK)}$(q)	**4E10 Fab SAH-MPER$_{(671\text{-}683KKK)}$(q)pSer**
Data collection		
Space group	$P6_122$	$P6_122$
Cell dimensions		
a, *b*, *c* (Å)	226.10, 226.10, 41.82	226.51, 226.51, 42.33
α, β, γ (°)	90.00, 90.00, 120.00	90.00, 90.00, 120.00
Resolution (Å)	48.95-2.91 (2.96-2.91) *	49.04-2.68 (2.75-2.68) *
R_{merge} (%) **	18.2 (66.6)	9.3 (59.7)
R_{pim}	4.2 (22.7)	2.1 (13.4)
$I/\sigma I$	16.4 (3.1)	28.0 (5.6)
Completeness (%)	95.6 (70.4)	99.9 (100)
Redundancy	21.9 (7.8)	20.7 (20.3)
Refinement		
Resolution (Å)	48.95-2.91	49.04-2.68
No. reflections	13,737 (501)	18,583 (1,335)
R_{work}/R_{free} (%)	21.0/26.8	17.0/22.2
No. atoms		
Protein	3,353	3,344
Peptide	150	162
PO_4 ion	5	0
TFA	14	0
Water	29	98
B factors (Å^2)		
Wilson plot	63.8	52.0
Protein	70.7	51.2
Peptide	81.1	59.8
Staple	75.0	48.5
PO_4 ion	110.5	-----
Dab-Gly-pSer	-----	105.6
Water	50.5	46.7
r.m.s. deviations		
Bond lengths (Å)	0.006	0.010
Bond angles (°)	0.79	1.34

* Values in parentheses are for highest-resolution shell.

** Data sets from two crystals were merged together for 4E10 Fab–SAH-MPER$_{(671\text{-}683KKK)}$(q) complex. A full data set was collected on one crystal for 4E10 Fab–SAH-MPER$_{(671\text{-}683KKK)}$(q)pSer complex.

Table 2

Data collection and refinement statistics for the 10E8 Fab–SAH-MPER$_{(662\text{-}683KKK)}$(B,q) complex

	10E8 Fab SAH-MPER$_{(662\text{-}683KKK)}$(B,q)
Data collection	
Space group	P 2_1 2_1 2_1
Cell dimensions	
a, *b*, *c* (Å)	68.6 126.3 129.9
α, β, γ (°)	90, 90, 90
Resolution (Å)	50-4.15 (4.25-4.15) *
R_{merge} (%)**	30.2 (56.4)
$I/\sigma I$	5.6 (2.9)
Completeness (%)	95.1 (83.3)
Redundancy	6.4 (5.1)
Refinement	
Resolution (Å)	40.05-4.20 (4.35 - 4.20)
No. reflections	8120 (624)
R_{work}/R_{free} (%)	24.32/27.53
No. atoms	
Protein	7025
Peptide	0
Water	0
B factors (Å^2)	
Protein	76.90
r.m.s. deviations	
Bond lengths (Å)	0.002
Bond angles (°)	0.60

* Values in parentheses are for highest-resolution shell.

** A full data set was collected on one crystal.